



Dalton  
Transactions

**Facile immobilization of  $P^{NN}NP$ -Pd pincer complexes in MFU-4l-OH and the effects of guest loading on Lewis acid catalytic activity**

Journal:	<i>Dalton Transactions</i>
Manuscript ID	DT-ART-11-2022-003781.R1
Article Type:	Paper
Date Submitted by the Author:	22-Dec-2022
Complete List of Authors:	Hilliard, Jordon; The Ohio State University, Chemistry and Biochemistry Wade, Casey; The Ohio State University, Chemistry and Biochemistry

SCHOLARONE™  
Manuscripts

## ARTICLE

# Facile immobilization of P<sup>N</sup>N<sup>N</sup>P-Pd pincer complexes in MFU-4l-OH and the effects of guest loading on Lewis acid catalytic activity

Jordon S. Hilliard and Casey R. Wade\*

Received 00th January 20xx,  
Accepted 00th January 20xx

DOI: 10.1039/x0xx00000x

A palladium diphosphine pincer complex H<sub>3</sub>(P<sup>N</sup>N<sup>N</sup>P-Pd) has been encapsulated in the benzotriazolite MOF MFU-4l-OH ([Zn<sub>5</sub>(OH)<sub>4</sub>(btdd)<sub>3</sub>], btdd<sup>2-</sup> = bis(1,2,3-triazolo)dibenzodioxin), and the resulting materials were investigated as Lewis acid catalysts for cyclization of citronellal to isopulegol. Rapid immobilization is facilitated by a Brønsted acid-base reaction between the P<sup>N</sup>N<sup>N</sup>P-Pd benzoic acid substituents and Zn–OH groups at the framework nodes. Catalyst loading can be controlled up to a maximum of 0.5 pincer complexes per formula unit [**Pdl-x**, Zn<sub>5</sub>(OH)<sub>4-nx</sub>(btdd)<sub>3</sub>(H<sub>3-n</sub>P<sup>N</sup>N<sup>N</sup>P-Pd)]<sub>x</sub> x = 0.06–0.5, n ≈ 2.75]. Oxidative ligand exchange was used to replace I<sup>-</sup> with weakly coordinating BF<sub>4</sub><sup>-</sup> anions at the Pd–I sites, generating the activated MOFs **PdBF<sub>4</sub>-x** (x = 0.06, 0.10, 0.18, 0.40). The Lewis acid catalytic activity of the **PdBF<sub>4</sub>-x** series decreases with increasing catalyst density as a result of the appearance of mass transport limitations. Initial catalytic rates show that the activity of **PdBF<sub>4</sub>-0.06** approaches the intrinsic activity of a homogeneous P<sup>N</sup>N<sup>N</sup>P-PdBF<sub>4</sub> catalyst analogue. In addition, **PdBF<sub>4</sub>-0.06** exhibits better catalytic activity than the metallolinker-based MOF Zr-PdBF<sub>4</sub> and was not subject to leaching or catalyst degradation processes observed for the homogeneous analogue.

## Introduction

Metal-organic frameworks (MOFs) have continued to attract considerable interest as heterogeneous supports for catalysis.<sup>1–6</sup> Their multifunctional structures offer a wide range of potential strategies for immobilizing well-defined molecular catalysts that can result in marked improvements in stability, activity, and/or selectivity compared to homogeneous analogues. Encapsulation is one of the most versatile immobilization strategies since it minimizes synthetic effort and potentially allows for the use of a range of different MOF supports. However, catalyst species often need to be confined in the pores to prevent leaching, and methods such as dynamic linker exchange and ion exchange have been developed to address these concerns.<sup>7,8</sup> For example, Chmielewski and co-workers have reported the encapsulation of an amine-tagged Hoveyda–Grubbs type olefin metathesis catalyst in MIL-101-SO<sub>3</sub>H via an acid-base reaction between the guest amines and sulfonic acid groups on the framework linkers.<sup>9</sup>

Recently, we reported the synthesis, characterization and catalytic activity of MOFs assembled from metallolinkers based on diphosphine pincer complexes.<sup>10–15</sup> Among these materials, a Zr MOF containing P<sup>N</sup>N<sup>N</sup>P-Pd metallolinkers (Zr-PdBF<sub>4</sub>) demonstrated good activity for the carbonyl–ene cyclization of citronellal to isopulegol upon oxidative ligand exchange to activate the Lewis acidic palladium center (Fig. 1).<sup>12</sup> Zr-PdBF<sub>4</sub> contains a very high density of catalytically active Pd sites (0.76 mmol/g, 8.1 wt%). However, owing to the nature of this framework, it is difficult to vary active site density or interrogate

the catalytic efficiency with respect to reactivity at bulk versus surface Pd sites.

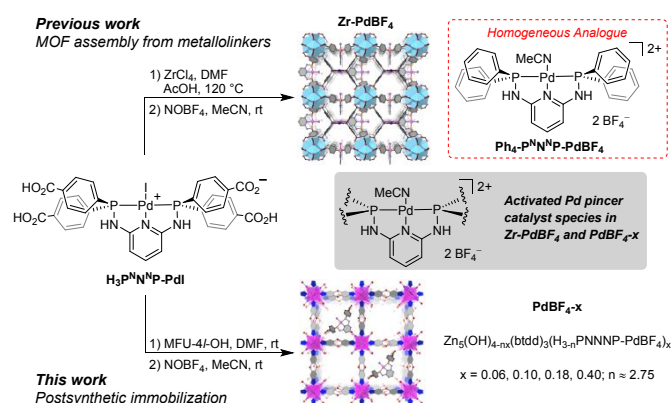


**Fig. 1** Metallolinker (Zr-PdBF<sub>4</sub>) and postsynthetic immobilization (PdBF<sub>4</sub>-x) approaches for MOF catalyst design with P<sup>N</sup>N<sup>N</sup>P-Pd complexes.

The ability of MOFs to support high densities of catalytically active sites is often touted as beneficial, but mass transport limitations can prevent MOF-based catalysts from attaining the intrinsic activity of the molecular catalyst species. Moreover, systematic studies evaluating the effects of immobilized catalyst density in MOFs have been scarce.<sup>16–20</sup> With this in mind, we sought to explore more versatile methods of immobilizing P<sup>N</sup>N<sup>N</sup>P-Pd catalyst species in MOFs to investigate the relationship between active site density and catalytic activity. Herein, we describe a rapid and convenient method for immobilizing P<sup>N</sup>N<sup>N</sup>P-Pd complexes in the Zn–OH functionalized MOF MFU-4l-OH.<sup>21,22</sup> This approach is similar to solvent assisted ligand incorporation (SALI) developed for Zr-based MOFs with under-coordinated metal nodes.<sup>23–26</sup> However, the

Department of Chemistry and Biochemistry, 100 West 18<sup>th</sup> Ave, The Ohio State University, Columbus, OH 43210, USA. E-mail: [wade.521@osu.edu](mailto:wade.521@osu.edu)

† Electronic supplementary information (ESI) available: Spectroscopic (NMR, XRF), crystallographic (PXRD), gas sorption, and GC-MS characterization. See DOI: 10.1039/x0xx00000x

use of the strongly basic Zn–OH functionalized MOF results in a facile postsynthetic acid-base reaction with carboxylic acid groups of the  $P^{N^N}NP$ -Pd complexes as well as tethering through multiple points of attachment.<sup>27</sup> The Lewis acid catalytic activities of the resulting materials have been evaluated for the carbonyl-ene cyclization of citronellal and kinetic studies show that diffusion limited behavior that can be ameliorated by reducing the  $P^{N^N}NP$ -Pd site density in the MOF.

## Results and discussion

### Synthesis and Characterization

MFU-4l-OH and  $H_3(P^{N^N}NP-Pd)$  were synthesized according to literature procedures.<sup>11,22</sup> A series of catalyst-loaded MOFs, **PdI-x** ( $Zn_5(OH)_{4-nx}(btdd)_3(H_{3-n}P^{N^N}NP-Pd)_x$ ,  $x = 0.06-0.5$ ) were prepared by treating MFU-4l-OH with DMF solutions containing varying amounts of  $H_3(P^{N^N}NP-Pd)$  (Fig. 1). In this formula,  $n$  defines the protonation state of the  $P^{N^N}NP$ -Pd complex and is dependent on the extent of the acid-base reaction with the Zn–OH groups at the MOF nodes (vide infra). It is also important to note that  $H_3(P^{N^N}NP-Pd)$  is a zwitterionic species in which a formal cationic charge on the Pd center is balanced by a deprotonated benzoate arm.<sup>11</sup> In all cases, guest adsorption is accompanied by complete dissipation of orange color from the solution and a color change of the MOF from beige to mustard yellow. The solid products were washed with DMF to remove any excess or weakly adsorbed pincer complex and subsequently solvent exchanged with acetonitrile. Powder X-ray diffraction (PXRD) analysis shows that the framework structure of the MOF is unchanged upon adsorption of the pincer complex (Fig. 2a). The amount of  $H_3(P^{N^N}NP-Pd)$  incorporated was quantified by integration of acid-digested  $^1H$  NMR spectra (Figs. S2–S6). The data reveal that the MOF quantitatively adsorbs  $H_3(P^{N^N}NP-Pd)$  up to a maximum loading of 0.50 equiv. per formula unit (Fig. S8). This maximum threshold is consistent with the alternating pore structure of MFU-4l-OH in which half of the cubic pores contain eight Zn–OH groups protruding from the corners (Type A) resulting in a pore diameter of  $\sim 12$  Å. The remaining cubic pores (Type B) do not contain exposed Zn–OH groups at their surface, resulting in a larger pore diameter of  $\sim 18$  Å (Figure S9). Accordingly, the empirical formula  $[Zn_5(OH)_{4-0.5n}btdd_3(H_{3-n}P^{N^N}NP-Pd)_{0.5}]$  represents a maximum loading of one pincer complex per Type A Zn–OH functionalized pore. A control experiment with MFU-4l-Cl, containing Zn–Cl rather than Zn–OH groups at the pore surface, resulted in negligible adsorption of  $H_3(P^{N^N}NP-Pd)$  under the same conditions (Fig. S8). The inability of  $H_3(P^{N^N}NP-Pd)$  to readily encapsulate in MFU-4l-Cl points the key role of the Zn–OH groups in facilitating adsorption of the carboxylic acid-functionalized complex via a Brønsted acid-base reaction.

$N_2$  adsorption isotherms measured for **PdI-0.06**, **PdI-0.16**, **PdI-0.40**, and the parent MFU-4l-OH show that  $N_2$ -accessible porosity and high internal surface areas are maintained with only modest decreases in capacity and calculated BET surface areas as a function of increased catalyst loading (Fig. 2b). The  $N_2$  adsorption isotherms were used to calculate the pore size

distribution using an infinite slit adsorption model with 2D-non-local density functional theory (2D-NLDFT).<sup>28</sup> The corresponding pore size distribution plots show decreasing volume for the Type A pores at 10–11 Å with increased catalyst loading, supporting immobilization of the complexes in this pore (Fig. S11).

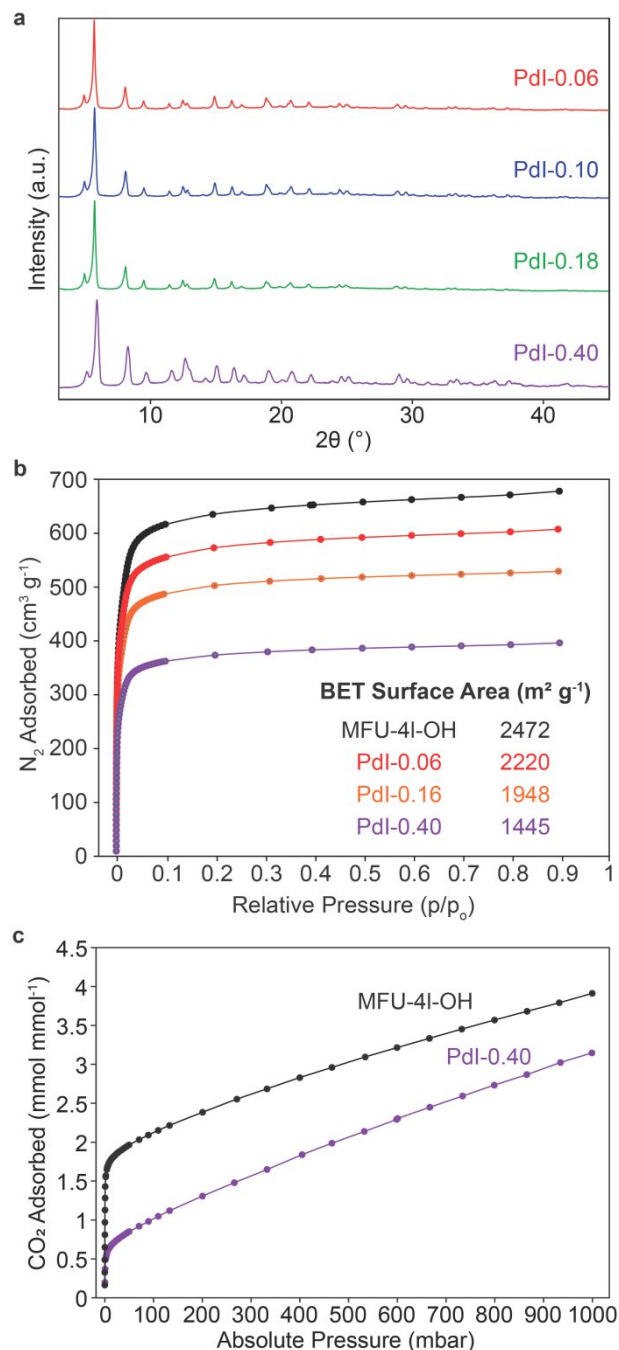


**Fig. 2** (a) PXRD patterns of PdI-x MOFs. (b)  $N_2$  adsorption isotherms measured for the PdI-x series of MOFs at 77 K after activation at 60 °C for 12 h. (c)  $CO_2$  adsorption isotherms measured for MFU-4l-OH and PdI-0.40 at 300 K.

$CO_2$  adsorption isotherms measured at 300 K show a significant decrease in low pressure adsorption for **PdI-0.40** in comparison to MFU-4l-OH (Fig. 2c). At 50 mbar, **PdI-0.40** and MFU-4l-OH adsorb 0.85 and 1.96  $mmol CO_2$  per  $mmol$  of MOF,

respectively. This decrease is consistent with quenching of  $\sim 1.1$  mmol of strong Zn–OH chemisorption sites per MOF formula unit and corresponds to acid-base reaction with  $\sim 2.75$  carboxylic acid groups per pincer complex. The nearly complete acid-base reaction of the  $H_3(P^{N^N}NP-PdI)$  complexes with the Zn–OH groups in **PdI-0.40** ( $Zn_5(OH)_{4-0.4n}btdd_3(H_{3-n}P^{N^N}NP-PdI)_{0.4}$ ,  $n = 2.75$ ) indicates that on average immobilization occurs via multiple points of attachment ( $>2$ ) to the MOF nodes. Indeed, the molecular structure of the  $P^{N^N}NP-PdI$  complex and MFU-4l pore diameter appear to be compatible with this scenario (Fig. S12).

The pincer-loaded MOFs **PdI-x** were treated with excess  $NOBF_4$  (4 equiv. per Pd) in acetonitrile to facilitate oxidative ligand exchange at the Pd–I sites and generate the corresponding **PdBF<sub>4</sub>-x** derivatives (Fig. 1). XRF analysis of the products indicates nearly quantitative exchange of  $I^-$  for  $BF_4^-$  (Fig. S13). Acid-digested  $^{31}P$  NMR spectra also show the disappearance of a resonance at 71 ppm associated with the  $[P^{N^N}NP-PdI]^+$  species and the appearance of two new signals at 72 ppm and 68 ppm corresponding to  $[P^{N^N}NP-Pd-MeCN]^{2+}$  and  $[P^{N^N}NP-Pd-OH]^+$  species, respectively (Fig. S14). The latter was previously observed upon acid digestion of Zr–PdBF<sub>4</sub>.<sup>12</sup> The  $^1H$  NMR spectra show all expected resonances for the pincer complexes while PXRD analysis confirms that the framework crystallinity is maintained (Figs. S15–S19).

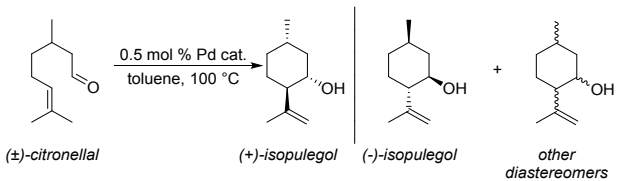
#### Catalytic Studies

The Lewis acid catalytic activity of the **PdBF<sub>4</sub>-x** series has been evaluated using the carbonyl-ene cyclization of citronellal (Table 1). This reaction has been used as a benchmark to establish the reactivity of MOFs containing Lewis acidic sites.<sup>29–38</sup> Zr–PdBF<sub>4</sub> was previously shown to exhibit good activity, providing 140 turnovers after 1 h at 0.5 mol % catalyst loading. Citronellal cyclization reactions with the **PdBF<sub>4</sub>-x** catalyst series were carried out under similar conditions (0.5 mol % Pd loading at 100 °C in toluene), and substrate conversion was monitored by GC-FID (Figs. S21–S24). The data reveal dramatic increases in catalytic activity with decreasing  $P^{N^N}NP-PdBF_4$  concentration in the MOF (Table 1 and Fig. 3). While **PdBF<sub>4</sub>-0.06** affords nearly quantitative substrate conversion after 1 h (TON = 190), less than 10 % conversion (TON = 16) is observed for **PdBF<sub>4</sub>-0.40** in the same period. Notably, **PdBF<sub>4</sub>-0.06** exhibits better catalytic activity for citronellal cyclization than that previously reported for Zr–PdBF<sub>4</sub> (Table 1, entry 5). Control reactions with MFU-4l–OH and MFU-4l–Cl showed  $< 5$  % citronellal conversion, supporting the immobilized Pd pincer complexes as the active species in the **PdBF<sub>4</sub>-x** catalysts (Table 1, entries 8 and 9).

PXRD and acid-digested  $^1H$  NMR spectra of **PdBF<sub>4</sub>-0.06** after the first catalytic run show no loss of framework crystallinity or decrease in Pd pincer complex loading in the MOF (Fig. S25–S26). Accordingly, **PdBF<sub>4</sub>-0.06** could be recycled up to three times without any significant loss in catalytic activity (Fig. S27). A hot filtration test with **PdBF<sub>4</sub>-0.18** also shows an abrupt halt of catalytic activity when the solid MOF was removed from the reaction after  $\sim 10$  % substrate conversion, supporting the heterogeneous nature of the catalyst (Fig. S29). Moreover, the observed trend in catalytic activity for the **PdBF<sub>4</sub>-x** catalyst

series is incongruent with leached Pd species being responsible for catalysis.

**Table 1.** Carbonyl-ene cyclization of citronellal.<sup>a</sup>



Entry	Catalyst	% Conv. <sup>b</sup>	TON <sup>c</sup>
1	<b>PdBF<sub>4</sub>-0.40</b>	8	16
2	<b>PdBF<sub>4</sub>-0.18</b>	32	64
3	<b>PdBF<sub>4</sub>-0.10</b>	78	156
4	<b>PdBF<sub>4</sub>-0.06</b>	95	190
5	Zr–PdBF <sub>4</sub> <sup>d</sup>	70	140
6	<sup>t</sup> Bu <sub>4</sub> –P <sup>N^N</sup> NP–PdBF <sub>4</sub> <sup>d</sup>	71 <sup>e</sup>	140 <sup>e</sup>
7	Ph <sub>4</sub> –P <sup>N^N</sup> NP–PdBF <sub>4</sub>	77	153
8	MFU-4l–OH	$< 5$	–
9	MFU-4l–Cl	$< 5$	–

<sup>a</sup> Reaction conditions: Substrate (0.4 mmol, 100 mM), catalyst (0.002 mmol Pd), toluene, 100 °C, 1 h. <sup>b</sup> Determined by GC-FID with respect to an internal standard (hexamethylbenzene) after 1 h. <sup>c</sup> Turnover numbers (TON) were calculated per Pd after 1 h. <sup>d</sup> From ref 12 <sup>e</sup> Reaction time of 3h

The **PdBF<sub>4</sub>-x** series shows good activity in comparison to other MOF-based Lewis acid catalysts that have been screened for carbonyl-ene cyclization of citronellal. In order to compare these catalysts, their activities are expressed here as mmol of substrate converted per gram of catalyst per hour (Fig. S30). A productivity of  $12.2 \text{ mmol} \cdot \text{g}_{\text{cat}}^{-1} \cdot \text{h}^{-1}$  is observed for **PdBF<sub>4</sub>-0.10**, which is considerably higher than that of **PdBF<sub>4</sub>-0.06** ( $9.16 \text{ mmol} \cdot \text{g}_{\text{cat}}^{-1} \cdot \text{h}^{-1}$ ). Thus, despite the higher TON per Pd observed for the latter, **PdBF<sub>4</sub>-0.10** is more efficient on a per mass basis. **PdBF<sub>4</sub>-0.10** and **PdBF<sub>4</sub>-0.06** are both more active than UiO-66-NO<sub>2</sub> ( $4.93 \text{ mmol} \cdot \text{g}_{\text{cat}}^{-1} \cdot \text{h}^{-1}$ ) which contains Lewis acidic Zr<sup>4+</sup> defect sites. However, the superacidic sulfonated framework, MOF-808-2.5SO<sub>4</sub>, shows the highest reported activity among MOF catalysts at  $83.1 \text{ mmol} \cdot \text{g}_{\text{cat}}^{-1} \cdot \text{h}^{-1}$ .<sup>34</sup> Zeolites containing Lewis acidic metal sites have also proven to be highly efficient catalysts for citronellal cyclization.<sup>36</sup> One of the most active reported zeolite catalysts, Sn-Beta provides an estimated productivity of  $341 \text{ mmol} \cdot \text{g}_{\text{cat}}^{-1} \cdot \text{h}^{-1}$  along with a high isopulegol product selectivity of  $> 80$  %.<sup>39</sup> Citronellal cyclization reactions typically produce a mixture of diastereomeric products among which isopulegol is the major component and most desirable product as a precursor to menthol.<sup>40</sup> All of the **PdBF<sub>4</sub>-x** catalysts yield a consistent isopulegol selectivity of 65 %, which is comparable to most reported Lewis acid catalysts and indicates that the MOF microenvironment does not prove any beneficial influence on product selectivity.<sup>41,42</sup>

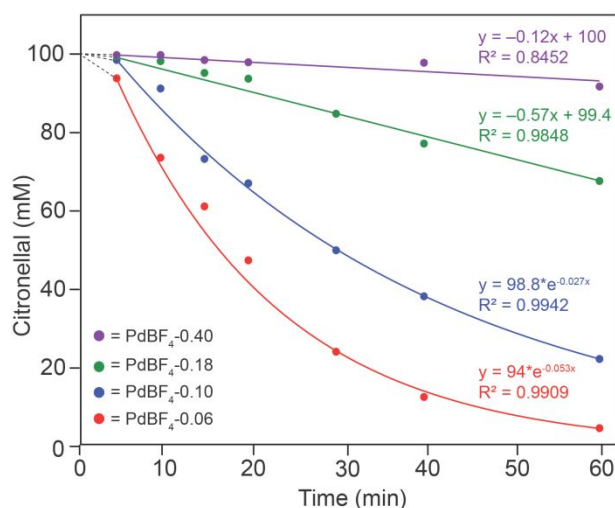


**Fig. 3** Kinetic profiles for the cyclization of citronellal using **PdBF<sub>4</sub>-x** catalysts. The lines are linear or exponential fits to the experimental data with the corresponding equations shown.

Substrate conversion was also monitored as function of time to gain further insight into the differences in catalytic activity among the **PdBF<sub>4</sub>-x** series (Fig. 3). Notably, a brief induction period of ~5 min is observed for all the **PdBF<sub>4</sub>-x** catalysts and is attributed to the time needed reach thermal equilibration at 100 °C. After this induction period, the kinetic profiles for **PdBF<sub>4</sub>-0.06** and **PdBF<sub>4</sub>-0.10** exhibit exponential decay indicative of first-order consumption of substrate. On the other hand, **PdBF<sub>4</sub>-0.18** and **PdBF<sub>4</sub>-0.40** show linear substrate conversion profiles consistent with pseudo-zero order kinetics. The evolving kinetic behavior of the **PdBF<sub>4</sub>-x** catalysts reflects the emergence of substrate and/or product diffusion limitations with increasing catalyst density in the MOF. This behavior is consistent with the immobilized **P<sup>N</sup>N<sup>N</sup>P-Pd** complexes blocking guest diffusion through the modestly sized Type A pores, which owing to the alternating pore structure, are a necessary pathway for accessing the bulk framework.

Mass transport is a key consideration in MOF catalyst design since hindered guest diffusion can obscure the intrinsic activity of catalytic sites and impose substrate size limits.<sup>43–45</sup> However, systematic evaluations of the effects of active site density and pore-clogging on catalytic activity are surprisingly uncommon for MOFs containing immobilized catalyst species.<sup>16–20</sup> Moreover, the relationship between catalyst density and activity varies considerably among the reported studies. For example, UiO-66 loaded with 25–40 wt% phosphotungstic acid (HPW) was studied for catalytic oxidation of cyclopentene to glutaraldehyde using H<sub>2</sub>O<sub>2</sub>, and a relatively high loading of 35 wt% HPW was found to be optimal.<sup>18</sup> Decreased product yield observed at higher catalyst loading was attributed to hindered mass transfer, but the decreased efficiency at lower loadings was not explained. On the other hand, Ott and coworkers immobilized a molecular H<sub>2</sub>-evolving catalyst, Fe<sub>2</sub>(cbdt)(CO)<sub>6</sub> (cbdt = 3-carboxybenzene-1,2-dithiolate), in MIL-101(Cr)-NH<sub>2</sub> at three different loadings: low (0.59 wt%), medium (2.35 wt%) and high (5.28 wt%).<sup>20</sup> Stoichiometric reduction experiments with cobaltocene gave direct insight into catalyst accessibility, showing improved

reduction yields for the low and medium loadings. However, all three materials exhibit similar TONs per catalyst site in photocatalytic hydrogen evolution screening, indicating that catalysis is not limited by reagent diffusion in the mesoporous framework. Consequently, although the change in activity for the **PdBF<sub>4</sub>-x** catalyst series may seem intuitive based on diffusion limitation considerations, such behavior is not necessarily innate to MOF-based catalysts.

The appearance of a shallow, linear kinetic profile with increased **P<sup>N</sup>N<sup>N</sup>P-Pd** site density in the **PdBF<sub>4</sub>-x** series suggests that catalysis occurs within the bulk of the MOF particles at low loadings, but gradually becomes restricted to active sites at or near the surface of the particles at high loadings. To further interrogate this hypothesis, we sought to compare the **PdBF<sub>4</sub>-x** catalysts with a homogeneous analogue that would provide information about intrinsic catalytic activity of the **P<sup>N</sup>N<sup>N</sup>P-PdBF<sub>4</sub>** species. <sup>t</sup>Bu<sub>4</sub>-**P<sup>N</sup>N<sup>N</sup>P-PdBF<sub>4</sub>** was previously evaluated for the carbonyl-ene cyclization of citronellal.<sup>12</sup> While this complex demonstrated good catalytic activity (Table 1, entry 6), it did not perform as well as the Zr-PdBF<sub>4</sub> MOF and was observed to decompose under catalytic conditions. Consequently, we decided to examine Ph<sub>4</sub>-**P<sup>N</sup>N<sup>N</sup>P-PdBF<sub>4</sub>** in the present study, considering that substitution of the tert-butyl benzoate groups with phenyl substituents might provide a more robust catalyst. Ph<sub>4</sub>-**P<sup>N</sup>N<sup>N</sup>P-PdBF<sub>4</sub>** provides 153 turnovers after 1 h, which is notably lower than the 190 turnovers observed for **PdBF<sub>4</sub>-0.06** under the same conditions but comparable to <sup>t</sup>Bu<sub>4</sub>-**P<sup>N</sup>N<sup>N</sup>P-PdBF<sub>4</sub>**. Ph<sub>4</sub>-**P<sup>N</sup>N<sup>N</sup>P-PdBF<sub>4</sub>** also provides similar isopulegol selectivity (65%) as the **PdBF<sub>4</sub>-x** MOF catalysts, confirming that MOF immobilization does not influence product selectivity. The full kinetic profile for Ph<sub>4</sub>-**P<sup>N</sup>N<sup>N</sup>P-PdBF<sub>4</sub>** could not be satisfactorily fit to a single first order exponential decay. Rather, it exhibits diminishing activity over the course of 1 h that is indicative of catalyst decomposition or deactivation (Fig. S31).

Excluding the brief induction period, Ph<sub>4</sub>-**P<sup>N</sup>N<sup>N</sup>P-PdBF<sub>4</sub>** exhibits a slightly higher initial rate (3.9 mM min<sup>-1</sup>) than **PdBF<sub>4</sub>-0.06** (3.0 mM min<sup>-1</sup>, Fig. 5a). This reveals that at the lowest loading in the series, some remnant mass transport limitations are still present, but **PdBF<sub>4</sub>-0.06** approaches the intrinsic catalyst activity of the **P<sup>N</sup>N<sup>N</sup>P-PdBF<sub>4</sub>** complex. Comparison across the **PdBF<sub>4</sub>-x** MOF series also shows a nearly linear decrease in initial rates up to **PdBF<sub>4</sub>-0.18** (Fig. 5b) This linear regime should reflect the decline in catalytic activity within the bulk of the MOF particles before an abrupt change to surface-limited reactivity at an approximate **P<sup>N</sup>N<sup>N</sup>P-Pd** loading of 0.20 per formula unit.

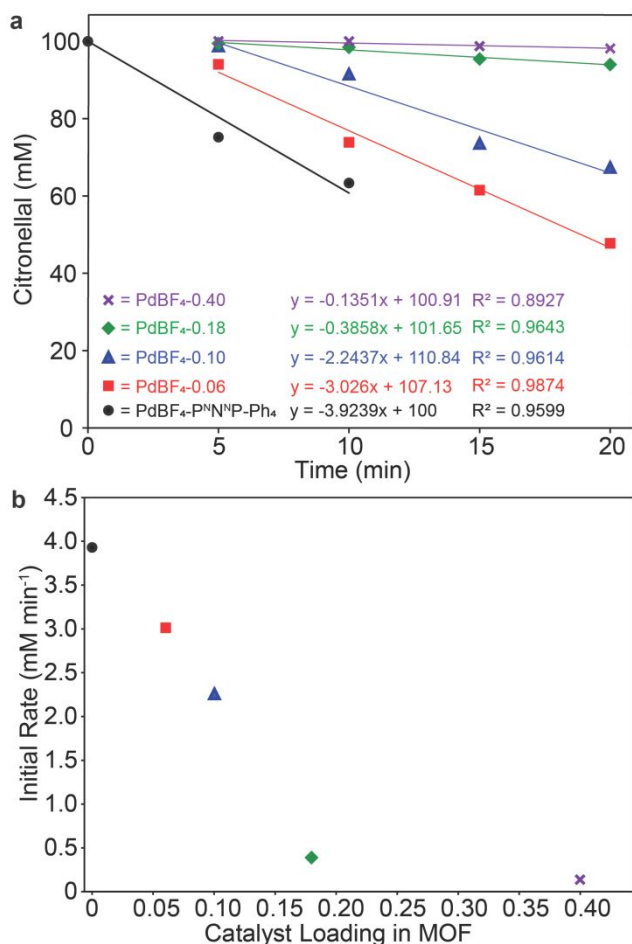


**Fig. 4** (a) Initial catalytic rates for the PdBF<sub>4</sub>-x MOF series and Ph<sub>4</sub>-P<sup>N</sup>N<sup>N</sup>P-PdBF<sub>4</sub>. (b) Initial rates from (a) plotted as a function of catalyst concentration in the MOF. The data point at catalyst loading = 0 corresponds to the homogeneous analogue Ph<sub>4</sub>-P<sup>N</sup>N<sup>N</sup>P-PdBF<sub>4</sub>.

## Conclusions

A postsynthetic X-type ligand exchange strategy has been used to immobilize carboxylic acid-functionalized P<sup>N</sup>N<sup>N</sup>P-Pd catalyst complexes in MFU-4l-OH via acid-base reaction at the Zn-OH sites of the metal nodes. This approach is similar to solvent assisted ligand incorporation (SALI) developed for Zr-based frameworks. However, the more basic MFU-4l-OH framework allows for precise control over catalyst loading under mild conditions and provides added stability via multipoint tethering of the catalyst complex in the functionalized micropores. As a result of its low catalyst site density, PdBF<sub>4</sub>-0.06 exhibits higher catalytic activity than the metal-linker-based MOF Zr-PdBF<sub>4</sub> and homogeneous analogue for the Lewis acid-catalyzed cyclization of citronellal. However, diffusion limited catalytic behavior emerges as the density of P<sup>N</sup>N<sup>N</sup>P-PdBF<sub>4</sub> complexes in the framework increases. The PdBF<sub>4</sub>-x catalysts could be recycled without loss in activity and displayed no apparent catalyst degradation or leaching. In addition, immobilization of the pincer complex inhibits the deactivation processes that plague the homogeneous analogues. Comparison of initial catalytic rates for the PdBF<sub>4</sub>-x and Ph<sub>4</sub>-P<sup>N</sup>N<sup>N</sup>P-PdBF<sub>4</sub> catalysts reveal that the activity of PdBF<sub>4</sub>-

0.06 approaches the intrinsic activity of the P<sup>N</sup>N<sup>N</sup>P-PdBF<sub>4</sub> species, but some mass transport effects are still present. These results further illuminate the relationships between heterogeneous catalyst activity, site density, and different immobilization strategies. Moreover, the facile encapsulation of H<sub>3</sub>(P<sup>N</sup>N<sup>N</sup>P-PdI) in MFU-4l-OH expands the range of methods available for heterogeneous catalyst design using immobilized molecular species and offers a complementary approach to SALI developed for Zr-based MOFs.

## Experimental section

### General considerations

All manipulations were carried out using a nitrogen-filled glovebox unless otherwise noted. N,N-dimethylformamide, acetonitrile, and toluene were degassed by sparging with ultra-high purity argon and passed through columns of drying agents using a Pure Process Technologies solvent purification system. (±)-Citronellal (96%) was purchased from Alfa Aesar and freshly distilled prior to use. NOBF<sub>4</sub> (98%) was purchased from Beantown Chemical and stored at low temp in an N<sub>2</sub>-filled glovebox. All other solvents and reagents were purchased from commercial suppliers and used as received unless otherwise noted. MFU-4l-OH and H<sub>3</sub>(P<sup>N</sup>N<sup>N</sup>P-PdI) were synthesized according to the reported procedures.<sup>11,22</sup> N<sub>2</sub> (77 K) and CO<sub>2</sub> (300 K) gas adsorption measurement were carried out using a Micromeritics 3Flex Adsorption Analyzer.

Powder X-ray diffraction patterns were measured using a Rigaku Miniflex 600 diffractometer with nickel-filtered Cu-Kα radiation (λ = 1.5418 Å). Solution-state NMR spectra were obtained using a Bruker AVIII 600 MHz NMR spectrometer with 180° water-selective excitation sculpting. XRF data for I<sup>-</sup>/BF<sub>4</sub><sup>-</sup> ligand exchange was obtained using an Innov-X Systems X-5000 spectrometer with a 50 KeV, 10W Tantalum X-ray tube.

### Synthesis of Pdl-x

A detailed procedure is given below for the synthesis of Pdl-0.06, and a similar procedure was used to prepare the other members of the Pdl-x (x = 0.10, 0.18, 0.40) catalyst series.

In an N<sub>2</sub>-filled glovebox, a vial containing MFU-4l-OH (0.107 g, 0.0899 mmol) was suspended in DMF (2 mL). The suspension was treated with a solution of H<sub>3</sub>(P<sup>N</sup>N<sup>N</sup>P-PdI) (4.8 mg, 0.0054 mmol) in DMF (2 mL). The vial was sealed, and the reaction mixture was gently stirred (100 rpm) for 2 h at room temperature. No immediate color change of the solution was observed, but the color gradually dissipated over the course of 2 h. The solid was collected by centrifugation and washed with DMF (2 × 15 mL) to ensure removal of any weakly adsorbed complex. The product was then solvent exchanged with MeCN (5 × 20 mL, 2 h per soak) to remove guest DMF molecules. The product was dried *in vacuo* at 60 °C to afford 86 mg of product. <sup>31</sup>P{<sup>1</sup>H} NMR (243 MHz, 3/1 v/v CF<sub>3</sub>COOH/DMSO-*d*<sub>6</sub>): δ 71.1 (s). Anal. calcd for chemical formula: [Zn<sub>5</sub>(OH)<sub>3.8</sub>btd<sub>3</sub>(H<sub>0.25</sub>P<sup>N</sup>N<sup>N</sup>P-PdI)<sub>0.07</sub> (C<sub>40.45</sub>H<sub>21.28</sub>I<sub>0.07</sub>N<sub>17.91</sub>O<sub>11.46</sub>P<sub>0.14</sub>Pd<sub>0.07</sub>Zn<sub>5</sub>): C, 37.7; H, 1.7; N, 20.4; Zn, 26.6; Pd, 0.60; Found: C, 37.40; H, 2.15; N, 19.43; Zn, 23.31; Pd, 0.48.

For the synthesis of **Pdl-x** ( $x = 0.10, 0.18, 0.40$ ), the amount of  $H_3(P^{N^N}P-Pdl)$  was varied according to the target catalyst loading. For samples with higher loadings (i.e. 0.40 equiv. per formula unit), extended reaction times up to 48 hours were required for complete dissipation of color from the solution.

#### Synthesis of **PdBF<sub>4</sub>-x**

A detailed procedure is given below for the synthesis of **PdBF<sub>4</sub>-0.06**, but similar procedures were used to prepare the other members of the **PdBF<sub>4</sub>-x** ( $x = 0.10, 0.18, 0.40$ ) catalyst series.

In an  $N_2$ -filled glovebox, a vial containing **Pdl-0.06** (86 mg, 0.069 mmol MOF, 0.004 mmol Pd) was suspended in MeCN (2 mL). A solution containing 4 equiv. NOBF<sub>4</sub> (2.0 mg, 0.017 mmol) in MeCN (3 mL) was added to the MOF suspension. The reaction was then stirred gently (100 rpm) at room temperature for 24 hours. The MOF was subsequently washed with MeCN (3 x 10 mL) and dried *in vacuo* at 60 °C to afford 78 mg of product. <sup>31</sup>P{<sup>1</sup>H} NMR (243 MHz, 3/1 v/v CF<sub>3</sub>COOH/DMSO-*d*<sub>6</sub>): δ 72.3 (s); 67.5 (s). For the synthesis of **PdBF<sub>4</sub>-x** ( $x = 0.10, 0.18, 0.40$ ), the amount of NOBF<sub>4</sub> in MeCN (3 mL) was varied according to the  $P^{N^N}P-Pdl$  loading.

#### Synthesis of **[Ph<sub>4</sub>-P<sup>N</sup>N<sup>N</sup>P-PdCl]Cl**

In an  $N_2$ -filled glovebox, a solution of Ph<sub>4</sub>-P<sup>N</sup>N<sup>N</sup>P (0.6513 g, 1.36 mmol) in 10 mL of THF was combined with PdCl<sub>2</sub>(cod) (0.3875 g, 1.36 mmol). The reaction was stirred vigorously for 12 hours resulting in a yellow-orange suspension. The resulting suspension was filtered in air to afford a bright yellow solid which was successively washed with THF (3 x 5 mL) and pentane (3 x 5 mL), then dried under reduced pressure to yield [Ph<sub>4</sub>-P<sup>N</sup>N<sup>N</sup>P-PdCl]Cl (0.7694 g, 86%). <sup>1</sup>H NMR (600 MHz, DMSO-*d*<sub>6</sub>): δ 10.75 (bs, 2H, NH), 7.91 (dd, 8H, <sup>3</sup>J<sub>H-P</sub> = 14.7 Hz, <sup>3</sup>J<sub>H-H</sub> = 6.7 Hz, *o*-phenyl H), 7.78 (t, 1H, <sup>3</sup>J<sub>H-H</sub> = 8.1 Hz, pyridine Ar-H), 7.68 (t, 4H, <sup>3</sup>J<sub>H-H</sub> = 7.4 Hz, *p*-phenyl H), 7.63 (t, 8H, <sup>3</sup>J<sub>H-H</sub> = 7.4 Hz, *m*-phenyl H), 6.72 (d, 2H, <sup>3</sup>J<sub>H-H</sub> = 8.1 Hz, pyridine H). <sup>31</sup>P{<sup>1</sup>H} NMR (243 MHz, DMSO-*d*<sub>6</sub>): δ 68.5 (s).

#### Synthesis of **[Ph<sub>4</sub>-P<sup>N</sup>N<sup>N</sup>P-Pdl]I**

A solution of [Ph<sub>4</sub>-P<sup>N</sup>N<sup>N</sup>P-PdCl]Cl (0.3479 g, 0.53 mmol) in 30 mL of MeCN was stirred vigorously while adding in a solution of NaI (0.1608 g, 1.07 mmol) in 10 of MeCN. Immediate formation of NaCl was observed and the reaction was allowed to proceed for 4 h with stirring at room temperature. The solvent was then removed under reduced pressure to afford a yellow-brown solid then washed successively with water (3 x 20 mL) and diethyl ether (3 x 5 mL). The solid was dried under reduced pressure to yield of [Ph<sub>4</sub>-P<sup>N</sup>N<sup>N</sup>P-Pdl]I (0.4090 g, 76%). <sup>1</sup>H NMR (600 MHz, DMSO-*d*<sub>6</sub>): δ 10.20 (bs, 2H, NH), 7.85 (m, 9H, *o*-phenyl H, pyridine Ar-H), 7.69 (t, 4H, <sup>3</sup>J<sub>H-H</sub> = 7.3 Hz, *p*-phenyl H), 7.64 (t, 8H, <sup>3</sup>J<sub>H-H</sub> = 7.5 Hz, *m*-phenyl H), 6.63 (d, 2H, <sup>3</sup>J<sub>H-H</sub> = 8.0 Hz, pyridine H). <sup>13</sup>C{<sup>1</sup>H} NMR (101 MHz, DMSO-*d*<sub>6</sub>): δ 160.2 (t, *J*<sub>C-P</sub> = 7.09 Hz, 2C, Ar), 144.3 (s, C, Ar), 133.4 (s, 4C, Ar), 133.2 (t, *J*<sub>C-P</sub> = 7.51 Hz, 8C, Ar), 130.2 (t, *J*<sub>C-P</sub> = 29.63 Hz, 4C, Ar), 129.8 (t, *J*<sub>C-P</sub> = 5.72 Hz, 8C, Ar), 100.8 (t, *J*<sub>C-P</sub> = 4.97 Hz, 2C, Ar). <sup>31</sup>P{<sup>1</sup>H} NMR (243 MHz, DMSO-*d*<sub>6</sub>): δ 73.4 (s).

#### Synthesis of **[Ph<sub>4</sub>-P<sup>N</sup>N<sup>N</sup>P-Pd(NCCH<sub>3</sub>)]<sub>2</sub>[BF<sub>4</sub>]<sub>2</sub>**

In an  $N_2$ -filled glovebox, a suspension of [Ph<sub>4</sub>-P<sup>N</sup>N<sup>N</sup>P-Pdl]I (0.1048 g, 0.13 mmol) in 3 mL CH<sub>2</sub>Cl<sub>2</sub> and 3 mL MeCN was

prepared and cooled to -24 °C in the glovebox freezer. A separate solution of NOBF<sub>4</sub> (0.0754 g, 0.65 mmol) in 3 mL MeCN was prepared and cooled as described above. After cooling for 30 minutes, the NOBF<sub>4</sub> solution was added dropwise to the [Ph<sub>4</sub>-P<sup>N</sup>N<sup>N</sup>P-Pdl]I solution. After slowly warming to room temperature a distinct color change from yellow-brown to dark red was observed in addition to complex dissolution of the complex. The reaction was stirred for 30 minutes then the solvent was removed *in vacuo*. The resulting solid was dissolved in CH<sub>2</sub>Cl<sub>2</sub> and filtered through a 0.45 μm PTFE syringe filter then dried under reduced pressure to afford [Ph<sub>4</sub>-P<sup>N</sup>N<sup>N</sup>P-Pd(NCCH<sub>3</sub>)]<sub>2</sub>[BF<sub>4</sub>]<sub>2</sub> as a red-orange solid (0.0955, 96%). <sup>1</sup>H NMR (600 MHz, CD<sub>3</sub>CN): δ 8.03 (bs, 2H, NH), δ 7.82 (dd, 8H, <sup>3</sup>J<sub>H-P</sub> = 14.6 Hz, <sup>3</sup>J<sub>H-H</sub> = 7.6 Hz, *o*-phenyl H), δ 7.78 (t, 4H, <sup>3</sup>J<sub>H-H</sub> = 7.5 Hz, *p*-phenyl H), δ 7.67 (m, 9H, *m*-phenyl H, pyridine Ar-H), δ 6.67 (d, 2H, <sup>3</sup>J<sub>H-H</sub> = 8.2 Hz, pyridine Ar-H). <sup>13</sup>C{<sup>1</sup>H} NMR (151 MHz, DMSO-*d*<sub>6</sub>): δ 161.8 (t, *J*<sub>C-P</sub> = 6.97 Hz, 2C, Ar), 146.0 (s, C, Ar), 135.0 (s, 4C, Ar), 133.6 (t, *J*<sub>C-P</sub> = 7.84 Hz, 8C, Ar), 130.8 (t, *J*<sub>C-P</sub> = 6.58 Hz, 8C, Ar), 128.4 (t, *J*<sub>C-P</sub> = 30.56 Hz, 4C, Ar), 103.1 (t, *J*<sub>C-P</sub> = 5.53 Hz, 2C, Ar). <sup>31</sup>P{<sup>1</sup>H} NMR (243 MHz, CD<sub>3</sub>CN): δ 76.9 (s).

#### General procedure for carbonyl-ene kinetic studies

In an  $N_2$ -filled glovebox, a 10 mL vial equipped with a 13mm PTFE silicone septa disk was charged with 0.5 mol % catalyst with respect to palladium, (±)-citronellal (0.4 mmol), toluene (4 mL), and a known amount of hexamethylbenzene as an internal standard. The reaction mixture was heated at 100 °C and aliquots were collected over a 60-minute period. Substrate conversion was determined by GC-FID. Recyclability studies were conducted for **PdBF<sub>4</sub>-0.06** over three cycles. **PdBF<sub>4</sub>-0.06** was isolated between cycles via centrifugation and washed with toluene (3 x 4 mL) before being resubjected to the reaction conditions outlined above.

#### Conflicts of interest

There are no conflicts to declare.

#### Acknowledgements

Acknowledgment is made to the National Science Foundation under Grant No. 2044904 for support of this research.

#### Notes and references

- 1 S. M. Cohen, Z. Zhang and J. A. Boissonnault, *Inorg. Chem.*, 2016, **55**, 7281–7290.
- 2 T. Drake, P. Ji and W. Lin, *Acc. Chem. Res.*, 2018, **51**, 2129–2138.
- 3 A. Bavykina, N. Kolobov, I. S. Khan, J. A. Bau, A. Ramirez and J. Gascon, *Chem. Rev.*, 2020, **120**, 8468–8535.
- 4 Y. S. Wei, M. Zhang, R. Zou and Q. Xu, *Chem. Rev.*, 2020, **120**, 12089–12174.
- 5 S. Kumar, B. Mohan, Z. Tao, H. You and P. Ren, *Catal. Sci. Technol.*, 2021, **11**, 5734–5771.
- 6 T. M. Rayer and C. R. Wade, in *Comprehensive Organometallic Chemistry IV*, Elsevier, 2022, pp. 257–284.

- 7 Z. Li, T. M. Rayder, L. Luo, J. A. Byers and C. K. Tsung, *J. Am. Chem. Soc.*, 2018, **140**, 8082–8085.
- 8 D. T. Genna, A. G. Wong-Foy, A. J. Matzger and M. S. Sanford, *J. Am. Chem. Soc.*, 2013, **135**, 10586–10589.
- 9 A. Chołuj, R. Karczykowski and M. J. Chmielewski, *Organometallics*, 2019, **38**, 3392–3396.
- 10 S. A. Burgess, A. Kassie, S. A. Baranowski, K. J. Fritzsing, K. Schmidt-Rohr, C. M. Brown and C. R. Wade, *J. Am. Chem. Soc.*, 2016, **138**, 1780–1783.
- 11 B. R. Reiner, N. T. Mucha, A. Rothstein, J. S. Temme, P. Duan, K. Schmidt-Rohr, B. M. Foxman and C. R. Wade, *Inorg. Chem.*, 2018, **57**, 2663–2672.
- 12 B. R. Reiner, A. A. Kassie and C. R. Wade, *Dalton Trans.*, 2019, **48**, 9588–9595.
- 13 A. A. Kassie, P. Duan, E. T. McClure, K. Schmidt-Rohr, P. M. Woodward and C. R. Wade, *Inorg. Chem.*, 2019, **58**, 3227–3236.
- 14 A. A. Kassie, P. Duan, M. B. Gray, K. Schmidt-Rohr, P. M. Woodward and C. R. Wade, *Organometallics*, 2019, **38**, 3419–3428.
- 15 A. A. Kassie and C. R. Wade, *Organometallics*, 2020, **39**, 2214–2221.
- 16 V. Pascanu, Q. Yao, A. Bermejo Gómez, M. Gustafsson, Y. Yun, W. Wan, L. Samain, X. Zou and B. Martín-Matute, *Chem. Eur. J.*, 2013, **19**, 17483–17493.
- 17 M. A. Nasalevich, R. Becker, E. V. Ramos-Fernandez, S. Castellanos, S. L. Veber, M. V. Fedin, F. Kapteijn, J. N. H. Reek, J. I. Van Der Vlugt and J. Gascon, *Energy Environ. Sci.*, 2015, **8**, 364–375.
- 18 X. L. Yang, L. M. Qiao and W. L. Dai, *Microporous Mesoporous Mater.*, 2015, **211**, 73–81.
- 19 K. M. Choi, D. Kim, B. Rungtaweeworanit, C. A. Trickett, J. T. D. Barmanbek, A. S. Alshammari, P. Yang and O. M. Yaghi, *J. Am. Chem. Soc.*, 2017, **139**, 356–362.
- 20 S. Roy, V. Pascanu, S. Pullen, G. González Miera, B. Martín-Matute and S. Ott, *Chem. Commun.*, 2017, **53**, 3257–3260.
- 21 A. M. Wright, Z. Wu, G. Zhang, J. L. Mancuso, R. J. Comito, R. W. Day, C. H. Hendon, J. T. Miller and M. Dincă, *Chem*, 2018, **4**, 2894–2901.
- 22 Z. Cai, C. E. Bien, Q. Liu and C. R. Wade, *Chem. Mater.*, 2020, **32**, 4257–4264.
- 23 P. Deria, W. Bury, J. T. Hupp and O. K. Farha, *Chem. Commun.*, 2014, **50**, 1965–1968.
- 24 P. Deria, J. E. Mondloch, E. Tylianakis, P. Ghosh, W. Bury, R. Q. Snurr, J. T. Hupp and O. K. Farha, *J. Am. Chem. Soc.*, 2013, **135**, 16801–16804.
- 25 P. Deria, W. Bury, I. Hod, C. W. Kung, O. Karagiari, J. T. Hupp and O. K. Farha, *Inorg. Chem.*, 2015, **54**, 2185–2192.
- 26 S. T. Madrahimov, J. R. Gallagher, G. Zhang, Z. Meinhart, S. J. Garibay, M. Delferro, J. T. Miller, O. K. Farha, J. T. Hupp and S. T. Nguyen, *ACS Catal.*, 2015, **5**, 6713–6718.
- 27 C. E. Bien, Z. Cai and C. R. Wade, *Inorg. Chem.*, 2021, **60**, 11784–11794.
- 28 C. Schlumberger and M. Thommes, *Adv. Mater. Interfaces*, 2021, **8**, 2002181.
- 29 L. Alaerts, E. Séguin, H. Poelman, F. Thibault-Starzyk, P. A. Jacobs and D. E. De Vos, *Chem. Eur. J.*, 2006, **12**, 7353–7363.
- 30 F. Vermoortele, M. Vandichel, B. Van De Voorde, R. Ameloot, M. Waroquier, V. Van Speybroeck and D. E. De Vos, *Angew. Chem. Int. Ed.*, 2012, **51**, 4887–4890.
- 31 F. G. Cirujano, F. X. Llabrés I Xamena and A. Corma, *Dalton Trans.*, 2012, **41**, 4249–4254.
- 32 F. Vermoortele, R. Ameloot, L. Alaerts, R. Matthesen, B. Carlier, E. V. R. Fernandez, J. Gascon, F. Kapteijn and D. E. De Vos, *J. Mater. Chem.*, 2012, **22**, 10313–10321.
- 33 F. Vermoortele, B. Bueken, G. Le Bars, B. Van De Voorde, M. Vandichel, K. Houthoofd, A. Vimont, M. Daturi, M. Waroquier, V. Van Speybroeck, C. Kirschhock and D. E. De Vos, *J. Am. Chem. Soc.*, 2013, **135**, 11465–11468.
- 34 J. Jiang, F. Gándara, Y. B. Zhang, K. Na, O. M. Yaghi and W. G. Klemperer, *J. Am. Chem. Soc.*, 2014, **136**, 12844–12847.
- 35 A. M. Rasero-Almansa, M. Iglesias and F. Sánchez, *RSC Adv.*, 2016, **6**, 106790–106797.
- 36 F. G. Cirujano, *Catal. Sci. Technol.*, 2017, **7**, 5482–5494.
- 37 F. G. Cirujano and F. X. Llabrés I Xamena, *J. Phys. Chem. Lett.*, 2020, **11**, 4879–4890.
- 38 M. Ermer, J. Mehler, B. Rosenberger, M. Fischer, P. S. Schulz and M. Hartmann, *ChemistryOpen*, 2021, **10**, 233–242.
- 39 A. Corma and M. Renz, *Chem. Commun.*, 2004, **4**, 550–551.
- 40 D. Dylong, P. J. C. Hausoul, R. Palkovits and M. Eisenacher, *Flavour Fragr. J.*, 2022, **37**, 195–209.
- 41 S. Serra, E. Brenna, C. Fuganti and F. Maggioni, *Tetrahedron Asymmetry*, 2003, **14**, 3313–3319.
- 42 T. K. Sarkar and S. K. Nandy, *Tetrahedron Lett.*, 1996, **37**, 5195–5198.
- 43 B. A. Johnson, A. M. Beiler, B. D. McCarthy and S. Ott, *J. Am. Chem. Soc.*, 2020, **142**, 11941–11956.
- 44 B. A. Johnson and S. Ott, *Chem. Sci.*, 2020, **11**, 7468–7478.
- 45 C. H. Sharp, B. C. Bukowski, H. Li, E. M. Johnson, S. Ilic, A. J. Morris, D. Gersappe, R. Q. Snurr and J. R. Morris, *Chem. Soc. Rev.*, 2021, **50**, 11530–11558.